# Rapid Fabrication of Designable Large-Scale Aligned Graphene Nanoribbons by Electro-hydrodynamic Nanowire Lithography

*Wentao Xu, Hong-Kyu Seo, Sung-Yong Min, Himchan Cho, Tae-Seok Lim, Chang-yeol Oh, Yeongjun Lee, and Tae-Woo Lee**

Graphene has superior electronic, physical, and chemical properties,[1–7] but its zero bandgap restricts many of its applications in future electronics.[8] However, the bandgap is expected to open when graphene is patterned into a narrow ribbon to confine carriers to a quasi-one-dimensional system.[9] Graphene nanoribbons (GNRs) that have a bandgap inversely proportional to the ribbon width are promising because they show significant gating effects;[10] they also have an enhanced on/off current ratio ($I_{on}/I_{off}$) at room temperature. GNRs were first fabricated using standard electron-beam lithography (EBL) with a hydrogen silsesquioxane mask, then etching graphene sheets with reactive oxygen plasma.[9] However, use of EBL is problematic because it is a serial process, and is time-consuming and expensive.[11] Furthermore, the narrowest GNR that can be produced using EBL is 12–20 nm, which is too wide to provide a sufficient bandgap for room-temperature field-effect transistors (FETs).[12] Other strategies for preparing GNRs include synthesizing them from solution,[13] longitudinally unzipping carbon nanotubes,[14–16] inorganic nanowire (i-NW) lithography,[17–19] and etching graphene sheets templated with diblock copolymers.[20–22] However, industrial applications of GNRs are still hampered by limitations to scalable fabrication and designable alignment of GNRs.

So far, only a few reliable methods have been developed for producing GNRs on a large scale while controlling the location and alignment of the GNRs. Scalable GNRs have been fabricated by thermally decomposing SiC[10] and by synthesizing them on Ni nanobars.[23] SiC is too costly to produce industrially, and decomposing SiC produces GNRs as wide as 40 nm, rendering this method impractical for producing narrow GNRs. The method of using Ni nanobars involves using EBL to pattern them, so the disadvantages of EBL cannot be avoided. Developing a simple method of producing GNRs remains challenging because of the complexity and limitations of currently-available methods of producing them.[24] Hence, an inexpensive, fast method of patterning and aligning GNRs on a large scale is required before fabricating circuits over large areas can become feasible.

Here, we demonstrate an innovative method of producing GNRs in large area: electro-hydrodynamic nanowire lithography (e-NW lithography). This method is fast and inexpensive, and can be used to fabricate GNRs on a large scale while designing their alignment. Although traditional i-NWs are expensive and their locations and alignments are difficult to control,[25] GNRs fabricated using e-NW lithography have great potential due to good controllability of position and orientation. Individually-controlled electro-hydrodynamically printed nanowires (e-NWs) were drawn at high speed on top of graphene, as physical masks to protect the underlying graphene during oxygen plasma etching. The number of nanowires and the spacing, length, and orientation of the nanowires were controllable because the nanowires were directly designed on the graphene instead of being transfer-printed onto the graphene surface. The circular cross-section of the e-NWs resulted in the formation of a nanoscale contact between the e-NWs and the underlying graphene: the resulting GNR width can be much smaller than the diameter of the e-NWs. The unprotected graphene was then etched with oxygen plasma, producing GNRs as narrow as ca. 9 nm. A graphene nanoribbon field-effect transistor (GNRFET) device showed a high $I_{on}/I_{off}$ of ca. 70 at room temperature and a hole mobility of ca. 300 $cm^2 V^{-1} s^{-1}$, which are indicative of an appreciable bandgap opening. Large-scale fabrication was achieved by patterning a GNRFET array consisting of 144 devices on a 4-inch silicon wafer.

Chemical vapor deposition (CVD) was used to synthesize a graphene sheet to the desired size on a copper foil. The graphene sheet was then transferred onto a 300 nm $SiO_2$/n+Si wafer (**Figure 1**). E-NWs whose alignment was designed were drawn on the graphene sheet as masks against oxygen plasma etching. Au electrodes were then patterned onto the masked graphene sheet, and the unprotected graphene was etched using oxygen plasma. The e-NWs can remain as a protective passivation layer on top of the GNR, or can be removed by brief sonication in chloroform.

Our home-built e-NW printer has two major components: an injector and a collector (Figure 1).[26] The injector ensures a hydrodynamic process similar to electrospinning, which uses electrostatic force to stretch a polymer solution in order to form NWs.[27,28] The collector is mounted horizontally and can move horizontally. The speed of the collector movement

Dr. W. Xu, H.-K Seo, S.-Y. Min, H. Cho, T.-S. Lim, Y. Lee, Prof. T.-W. Lee
Department of Materials Science and Engineering
Pohang University of Science and Technology (POSTECH)
Pohang, Gyungbuk 790–784, Republic of Korea
E-mail: twlee@postech.ac.kr
C.-y Oh
National Institute for Nanomaterials Technology
Pohang University of Science and Technology (POSTECH)
Pohang, Gyungbuk 790–784, Republic of Korea

**DOI: 10.1002/adma.201306081**

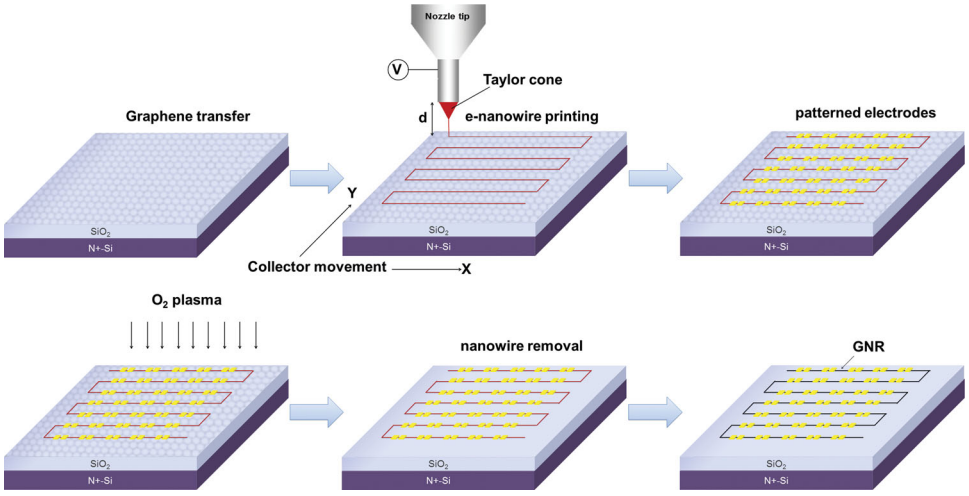


**Figure 1.** Schematic of process used to fabricate the large-scale GNRFET array, including graphene transfer, e-NW printing, electrode patterning, oxygen plasma etching, nanowire removal, and the final GNRFET array.

can be adapted to the speed at which the NWs are printed onto the collector. Straight, continuous e-NWs can be produced by adjusting parameters such as the concentration of polymer in the solution, the injection rate, the voltage, the nozzle-to-collector distance, and the speed at which the collector moves. The designed alignment of the e-NWs can be obtained by digitally controlling the movement of the collector. Continuous polyvinyl carbazole (PVK) nanowires were formed and were aligned in parallel at a constant pitch of 50 or 20 µm (**Figure 2**a,b). The solid-state NWs had a perfectly circular cross-section,[26] which ensured a very narrow contact region between the e-NWs and the underlying graphene sheet. The nozzle-to-collector distance $d$ is very important because the PVK jet should arrive as a solid NW at the substrate while maintaining the straight-jet region within a few millimeter (The NW printing optimum distance ($d_o$) is depending on the solution); when $d$ is smaller than a $d_o$, the PVK arrives as a liquid and then rapidly merge without forming solid-state NWs; when $d$ is larger than $d_o$, the PVK stream arrives as a solid at the substrate but forms coiled NWs. When a solution of 3.77 wt% PVK dissolved in styrene was used, $d \approx 2.5$ mm. E-NW printing is fast and can be used to draw a uniform, continuous long wire. For example, a solution containing 3.77 wt% PVK dissolved in styrene was used to draw a 15-m-long continuous e-NW with a uniform diameter of ca. 310 nm (Figure 2g) at 8000 mm $min^{-1}$ in <2 min. Several other typical e-NW alignments such as grids (Figure 2c), ladders (Figure 2d), and stars (Figure 2e) were drawn by digitally adjusting the collector movement. The diameters of the e-NWs were ca. 430, 310, 140, 65, and 45 nm when we used solutions containing 4.97, 3.77, 2.80, 2.05, and 1.80 wt% PVK dissolved in styrene, respectively (Figures 2f–j). We found a linear relationship between the logarithm of the average e-NW diameter and the logarithm of the concentration of PVK in the solution (Figure S1, Supporting Information), implying that e-NWs could be fabricated with any diameter in the range 45–500 nm by adjusting the concentration of PVK in the solution.

The e-NWs act as masks against oxygen plasma etching. The aligned patterns of printed e-NWs were transferred to the underlying GNRs with oxygen plasma etching for 6 s (Figure 2k–o). We used a solution of 3.77 wt% PVK dissolved in styrene to draw continuous e-NWs with a uniform diameter of ca. 310 nm (Figure 2g). E-NWs and GNRs were etched for 6, 12, 24, and 36 s at 30 W; the diameter of the e-NWs, the width of the GNRs, and the narrowest region of the GNRs decreased exponentially as etching time increased (**Figure 3**a). Oxygen plasma treatment must be performed at power levels sufficiently low to enable etching to proceed mildly and under control.[11] The first 6 s of oxygen plasma etching were anisotropic and produced GNRs whose widths were similar to the diameters of the e-NWs. Extended exposure to oxygen plasma caused severe lateral etching in the shadow region and generated narrow GNRs. GNRs that are narrow enough to open a bandgap are demanded for circuit applications. Etching for 24 s reduced the average width of the GNR, and the narrowest region in the continuous GNR was determined to be ca. 9 nm from an AFM image (Figure 3b and Figure S4, Supporting Information). The GNR has average width of 16.05 nm and standard deviation $\sigma \approx 2.65$ nm.[29]

Raman spectroscopy was used to analyze the graphene before and after etching (Figure 3c–f). The Raman spectrum for pristine graphene (Figure 3d) included a 2D peak at 2685 $cm^{-1}$ caused by second-order zone boundary photons, a G peak at ca. 1590 $cm^{-1}$ caused by in-plane optical vibration (i.e., the degenerate zone center of the $E_{2g}$ mode), and a D peak at ca. 1350 $cm^{-1}$ due to first-order zone boundary photons. The D peak is absent from the Raman spectrum for defect-free graphene, but is present in the Raman spectra for the graphene containing defects. The Raman spectrum for GNR region A (Figure 3c) was recorded. An additional strong D-band rose at 1345 $cm^{-1}$ in the Raman spectrum for GNR (Figure 3d) because of irregular edge disorders and oxidized dangling bonds in the GNR.[11,30] The intensity of the D peak depends on the structure of the edges in GNR: it is weak at zigzag edges and strong at armchair ones.[11] The disappearance of the 2D and G peaks (Figure 3d) at the unprotected region (B in Figure 3c) implies that the graphene had been efficiently removed: this is further supported by the Raman G mapping (Figure 3e), Raman 2D mapping (Figure 3f), and Raman D mapping (Figure S5, Supporting

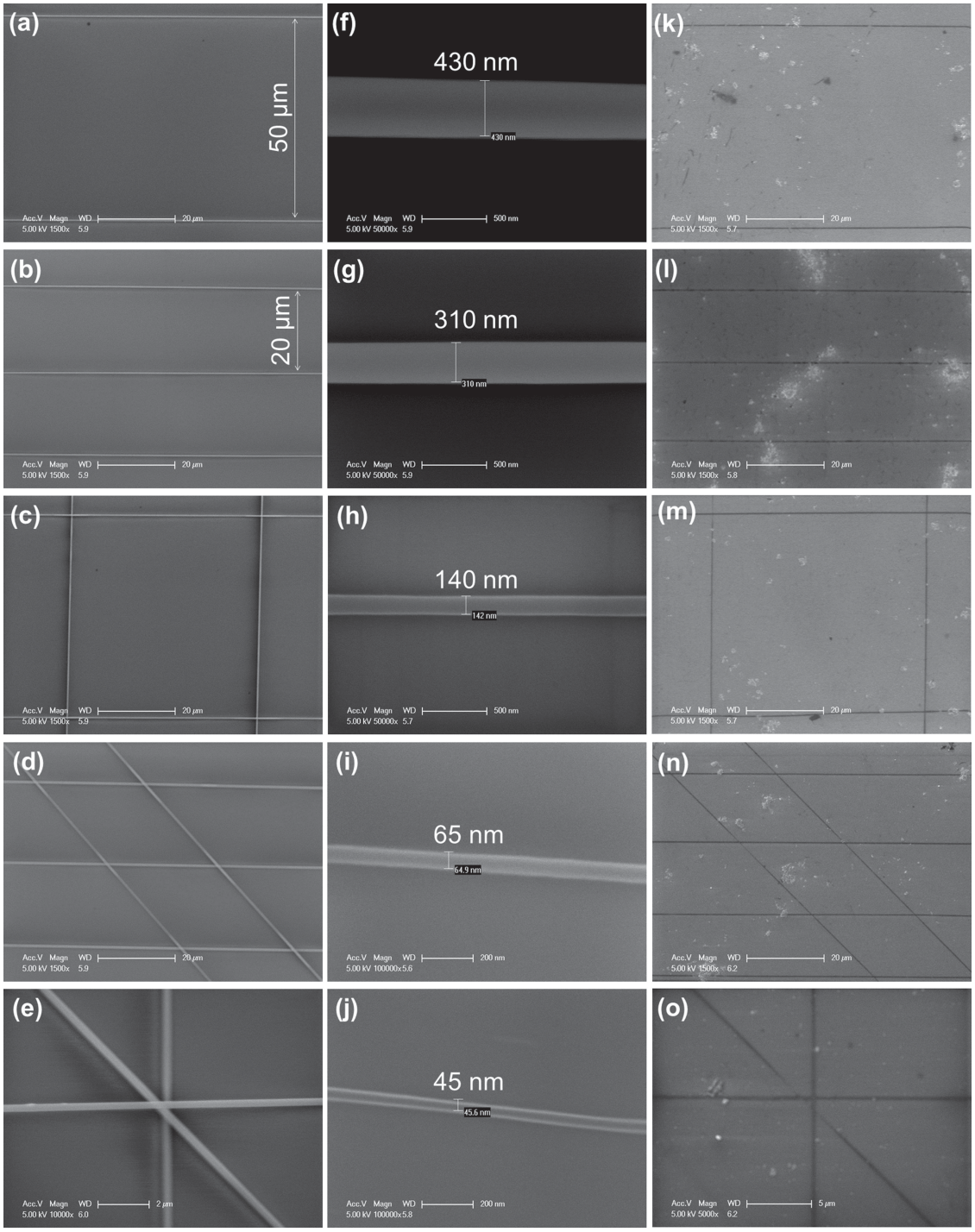


**Figure 2.** SEM images showing some typical examples of e-NW alignments including parallel lines at pitches of 50 µm (a) and 20 µm (b), grids (c), ladders (d), and stars (e); e-NWs fabricated with various diameters, drawn from solutions containing 4.98 (f), 3.77 (g), 2.80 (h), 2.05 (i), and 1.80 wt% (j) PVK dissolved in styrene; GNR architectures converted from the e-NW alignments (a)-(e) including parallel lines at pitches of 50 (k) and 20 µm (l), grids (m), ladders (n), and stars (o).

Information) for the framed region in Figure 3c. The $O_2$ plasma produced GNR with no crystallographically defined edge states.[11,31–34]

Most previous reports[13–15,17] on fabricating GNRFETs describe the use of short channels (i.e., several hundreds of nanometers to several micrometers long) and expensive and time-consuming EBL for patterning the electrodes because of the lack of continuous, long GNRs and the difficulty in aligning them. We fabricated GNRFET devices (**Figure 4**a) with a 50-µm-long channel using continuous GNRs produced from

ADVANCED MATERIALS
www.advmat.de

www.MaterialsViews.com

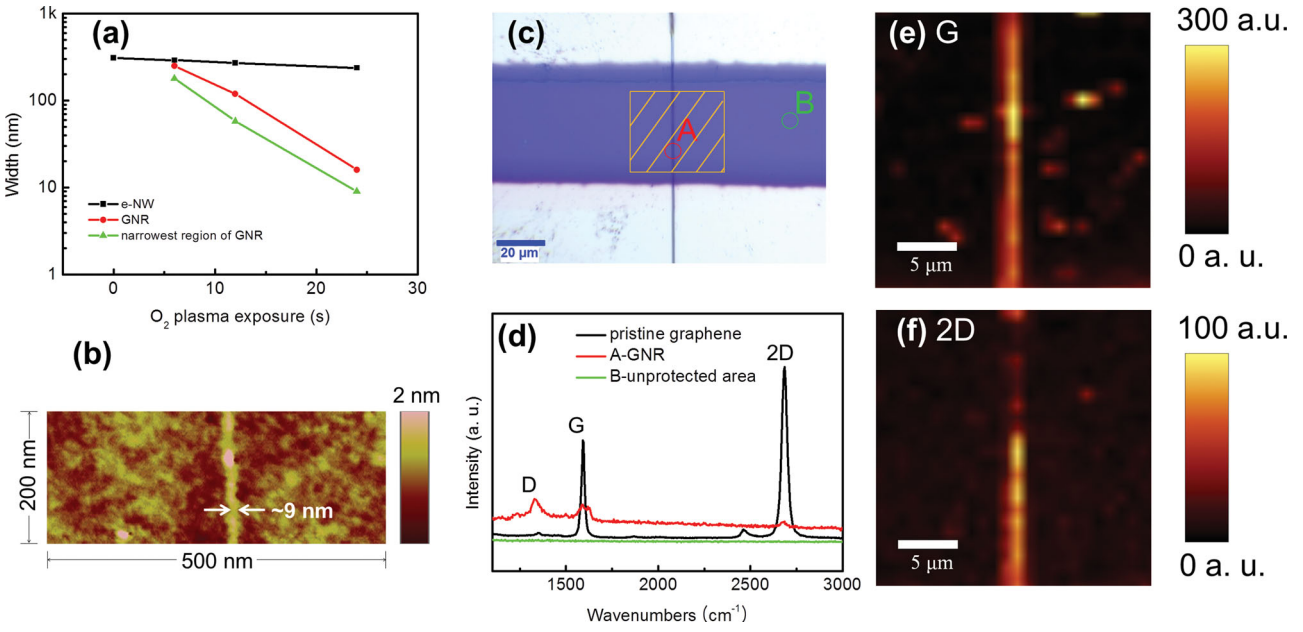


**Figure 3.** a) e-NW diameter, average GNR width, and the width of the narrowest region of the GNR plotted as functions of oxygen plasma etching time. b) AFM image with a ca. 9-nm region in the GNR etched for 24 s. c) OM image of a GNR across a 50-μm-wide gap (A, Raman-scanned region of GNR; B, unprotected area). d) Raman spectra for pristine graphene (in black), the GNR region A (in red), and the unprotected area B (in green) in (c). e) G-mapping for the framed region in (c). f) 2D mapping for the framed region in (c).

long, continuous, uniform e-NWs; hence, GNRFET devices can be produced rapidly and inexpensively.

The source–drain current $I_{sd}$ of the GNRFET device was plotted as a function of source–drain voltage $V_{sd}$ at various gate voltages $V_g$ (Figure 4b); the device delivered an on-current of ca. 1.50 μA at $V_{sd} = -0.1$ V and $V_g = -60$ V. $I_{sd}$ was plotted against $V_g$ for GNRFET devices etched with oxygen plasma for various lengths of time (Figure 4c). The as-transferred graphene exhibited a weak gate effect, showing an almost constant $I_{sd} \approx$ 650 μA ($V_{sd} = -0.01$ V). The device fabricated from GNRs etched for 12 s exhibited a clear p-type field effect with $I_{on}/I_{off} \approx 5$. The GNRs became progressively thinner and the width of the narrowest region of the GNR decreased to ca. 9 nm with increasing etching time to 24 s (Figure 3b). $I_{on}/I_{off}$ for the device fabricated

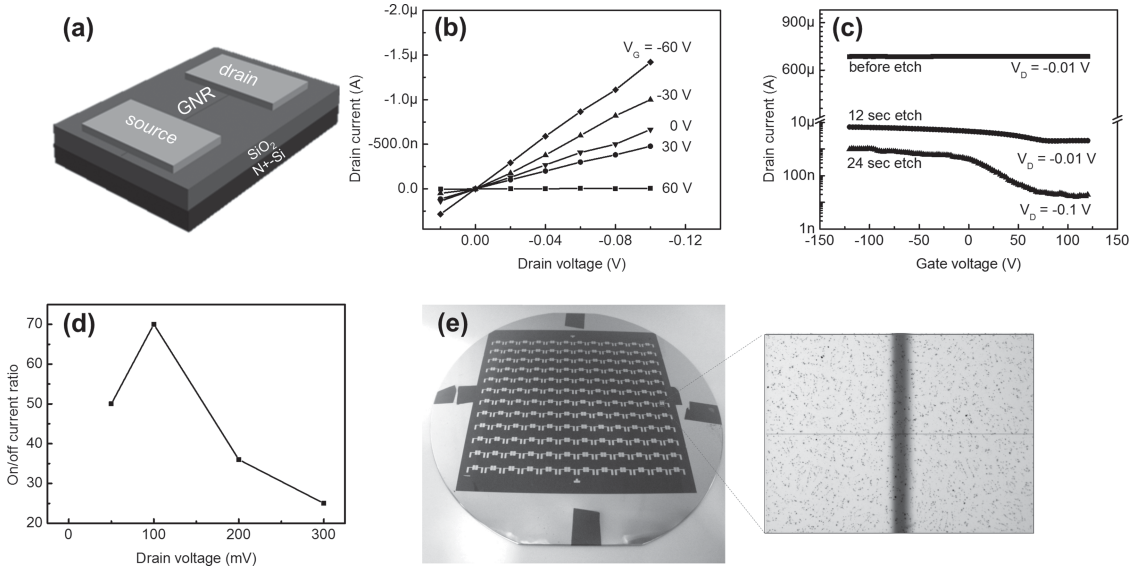


**Figure 4.** a) Schematic of a GNRFET device. b) Typical output characteristics of a GNRFET fabricated from GNRs etched for 24 s. c) Typical transfer characteristics of GNRFETs fabricated from GNRs etched for 0, 12, and 24 s. d) On/off current ratio plotted as a function of drain voltage for a GNRFET fabricated from GNRs etched for 24 s to indicate a bandgap of ca. 100 meV. e) Array consisting of 144 GNRFET devices fabricated on a 4-inch silicon wafer, and an amplified OM image of the channel region fabricated with an e-NW passivation layer.

from the GNRs etched for 24 s increased to ca. 70, which suggest appreciable bandgap opening at room temperature[8,10,23] Although etching GNRs for >24 s is expected to further narrow them, we found that over-etching GNRs caused the electrical pathways of the GNRs to partially break, dramatically sacrificing the on-state conductivity of the GNRFET devices.[11]

To further evaluate electrical properties, the carrier mobility $\mu$ of the device was calculated as:[35]

$$\mu = \frac{L}{W} C_g V_{sd} \frac{\Delta I_{sd}}{\Delta V_g} \quad (1)$$

where $C_g$ is the gate capacitance of the device per unit area, $L$ = 50 μm is channel length, and $W$ is the average width of the GNR. Hole mobility $\mu_h \approx 1300$ cm$^2$ V$^{-1}$ s$^{-1}$ for the device fabricated from the GNRs etched for 12 s, and $\mu_h \approx 300$ cm$^2$ V$^{-1}$ s$^{-1}$ for the device fabricated from the GNRs etched for 24 s. The decrease in $\mu$ as a result of the opening of the band gap of GNR was reported,[36] which would be the primary reason for the decrease in $\mu_h$ with decrease in GNR width. When the GNR width was decreased, the device based on the narrower GNR exhibited p-type transistor behavior (Figure 4c) because of p-doping due to edge oxidation and surface adsorbates.[19,37–39] A bandgap was opened because of the enhanced confinement of carriers in the transverse direction and because of the edge effect: the bandgap is inversely proportional to the width $W$ of the GNR, as described by the scaling relation $E_{gap} = \alpha/(W - W^*)$.[9] Here $\alpha$ and $W - W^*$ can be interpreted as the GNR sheet conductivity and the active GNR width participating in charge transport, respectively. The room-temperature $I_{on}/I_{off}$ reached a maximum of ca. 70 at $V_{sd}$ = 100 mV (Figure 4d), suggesting that the GNR has $E_{gap} \approx 100$ meV.[17] A 4-inch wafer-scale GNRFET array consisting of 144 devices was fabricated (Figure 4e). A 7 cm × 7 cm graphene sheet consisting of a high-quality mixture of single- and double-layer graphene with small faction of defects (Raman spectroscopy; D/G < 0.1) was transferred onto a 30-nm $SiO_2$/n+Si wafer (Figure S2, S3, Supporting Information). The mixture of single- and double-layer graphene was also confirmed by the height measurement of the GNR (Figure S4, Supporting Information). Aligned long e-NWs were drawn on the graphene sheet, followed by oxygen plasma treatment. The 50-μm channel regime consisted of a protective layer of PVK NWs and the underlying GNRs (Figure 4e).

In conclusion, we used e-NW lithography to demonstrate a rapid, low-cost fabrication of GNRs on a large scale while controlling their location and alignment. This new simple method of fabricating GNRs is versatile and shows great promise for fabricating large-area networks of ordered GNRs and other interesting GNR-based architectures including parallel lines, grids, ladders, and stars. A sub-10-nm GNR that showed a bandgap opening was obtained. Room-temperature electrical transport analysis was performed on a long-channel GNRFET device. The results indicate that the GNRFET exhibited p-type electrical characteristics, an on/off current ratio of ca. 70, and a hole mobility of ca. 300 cm$^2$ V$^{-1}$ s$^{-1}$. We envision that this method of fabricating GNRs in large area may open a new avenue for developing integrated GNRs for future circuits in graphene-based nanoelectronics.

## Experimental Section

*Graphene Synthesis and Device Fabrication*: Copper foils (99.8% purity, 25 μm thick, Alfa Aesar) were inserted into a quartz tube and heated to 1000 °C at 0.1 Torr under 16-sccm $H_2$ flow for 30 min, then a $CH_4$/$H_2$ (26 sccm/15 sccm) reaction gas mixture was allowed to flow over the foil for another 30 min, and the apparatus was then cooled to room temperature. A PMMA-assisted wet-transfer method was used to transfer the synthesized graphene sheet onto a 300-nm-thick $SiO_2$/n+Si substrate. Aligned polyvinyl carbazole (PVK) nanowires (NWs) were deposited using e-NW printing. Au 60-nm/Ti 3-nm source–drain electrodes were patterned through shadow masks on the graphene sheet. Oxygen plasma (BCS5004, SNTEK) (30 W, 0.2 Torr) was then applied to selectively etch the unprotected graphene region to produce GNRs.[40]

*Electro-hydrodynamic-Nanowire Fabrication*: A solution of PVK ($M_w \approx$ 1 100 000 g mol$^{-1}$, Aldrich) (3.77%) dissolved in styrene was injected through a metal nozzle at a feed rate of 550 nL min$^{-1}$. The nozzle-to-collector distance was 2.5 mm, and 3.6 kV was applied to the nozzle. The solution feed rate, nozzle-to-collector distance, and the voltage were adjusted for various concentrations of PVK solution. The syringe (Hamilton 1000 series) used for e-NW printing has a diameter of 4.61 mm and a capacity of 1 mL.

*Measurements*: SEM imaging was performed using a JEOL-6500 field-emission microscope. Raman spectroscopy was performed using a confocal Raman microscope (Alpha 300R, WITEC). AFM images were obtained using a Dimension 3100 microscope (Digital Instruments). The electrical transport properties were tested using a probe station in an $N_2$-filled glove box. The current–voltage data were collected using a Keithley 4200 semiconductor parameter analyzer.

## Supporting Information

Supporting Information is available from the Wiley Online Library or from the author.

## Acknowledgements

This work was supported by a grant (Code No.2013M3A6A5073175) from the Center for Advanced Soft Electronics under the Global Frontier Research Program of the Ministry of Science, ICT & Future Planning, Korea. This research was also supported by the Basic Research Program through the National Research Foundation (NRF) of Korea, funded by the Ministry of Education (NRF-2013R1A1A2012660), Korea.

Received: December 12, 2013
Revised: January 16, 2014
Published online: April 9, 2014

[1] K. S. Novoselov, A. K. Geim, S. V. Morozov, D. Jiang, Y. Zhang, S. V. Dubonos, I. V. Grigorieva, A. A. Firsov, *Science* **2004**, *306*, 666.
[2] F. Schwierz, *Nature* **2011**, *472*, 41.
[3] L. Ma, J. Wang, F. Ding, *ChemPhysChem* **2013**, *14*, 47.
[4] a) T.-H. Han, Y. Lee, M.-R. Choi, S.-H. Woo, S.-H. Bae, B. H. Hong, J.-H. Ahn, T.-W. Lee, *Nat. Photonics* **2012**, *6*, 105; b) H. Kim, S.-H. Bae, T.-H. Han, K.-G. Lim, J.-H. Ahn, T.-W. Lee, *Nanotechnology* **2014**, *25*, 014012.
[5] S.-J. Byun, H. Lim, G.-Y. Shin, T.-H. Han, S. H. Oh, J.-H. Ahn, H. C. Choi, T.-W. Lee, *J. Phys. Chem. Lett.* **2011**, *2*, 493.
[6] S. Bae, H. Kim, Y. Lee, X. Xu, J.-S. Park, Y. Zheng, J. Balakrishnan, T. Lei, H. R. Kim, Y. I. Song, Y.-J. Kim, K. S. Kim, B. Özyilmaz, J.-H. Ahn, B. H. Hong, S. Iijima, *Nat. Nanotechnol.* **2010**, *5*, 574.

[7] Z. Yan, J. Lin, Z. Peng, Z. Sun, Y. Zhu, L. Li, C. Xiang, E. L. Samuel, C. Kittrell, J. M. Tour, *ACS Nano* **2012**, *6*, 9110.
[8] I. Martin-Fernandez, D. Wang, Y. Zhang, *Nano Lett.* **2012**, *12*, 6175.
[9] M. Y. Han, B. Özyilmaz, Y. Zhang, P. Kim, *Phys. Rev. Lett.* **2007**, *98*, 206805.
[10] M. Sprinkle, M. Ruan, Y. Hu, J. Hankinson, M. Rubio-Roy, B. Zhang, X. Wu, C. Berger, W. A. de Heer, *Nat. Nanotechnol.* **2010**, *5*, 727.
[11] L. Liu, Y. Zhang, W. Wang, C. Gu, X. Bai, E. Wang, *Adv. Mater.* **2011**, *23*, 1246.
[12] W. S. Hwang, K. Tahy, X. Li, H. Xing, A. C. Seabaugh, C. Y. Sung, D. Jena, *Appl. Phys. Lett.* **2012**, *100*, 203107.
[13] X. Li, X. Wang, L. Zhang, S. Lee, H. Dai, *Science* **2008**, *319*, 1229.
[14] D. V. Kosynkin, A. L. Higginbotham, A. Sinitskii, J. R. Lomeda, A. Dimiev, B. K. Price, J. M. Tour, *Nature* **2009**, *458*, 872.
[15] L. Jiao, L. Zhang, X. Wang, G. Diankov, H. Dai, *Nature* **2009**, *458*, 877.
[16] L. Jiao, X. Wang, G. Diankov, H. Wang, H. Dai, *Nat. Nanotechnol.* **2010**, *5*, 321.
[17] J. Bai, X. Duan, Y. Huang, *Nano Lett.* **2009**, *9*, 2083.
[18] L. Liao, J. Bai, Y.-C. Lin, Y. Qu, Y. Huang, X. Duan, *Adv. Mater.* **2010**, *22*, 1941.
[19] A. Sinitskii, J. M. Tour, *Appl. Phys. Lett.* **2012**, *100*, 103106.
[20] J. Bai, X. Zhong, S. Jiang, Y. Huang, X. Duan, *Nat. Nanotechnol.* **2010**, *5*, 190.
[21] J. Y. Kim, B. H. Kim, J. O. Hwang, S.-J. Jeong, D. O. Shin, J. H. Mun, Y. J. Choi, H. M. Jin, S. O. Kim, *Adv. Mater.* **2013**, *25*, 1331.
[22] B. H. Kim, D. H. Lee, J. Y. Kim, D. O. Shin, H. Y. Jeong, S. Hong, J. M. Yun, C. M. Koo, H. Lee, S. O. Kim, *Adv. Mater.* **2011**, *23*, 5618.
[23] T. Kato, R. Hatakeyama, *Nat. Nanotechnol.* **2012**, *7*, 651.
[24] G. Xie, Z. Shi, R. Yang, D. Liu, W. Yang, M. Cheng, D. Wang, D. Shi, G. Zhang, *Nano Lett.* **2012**, *12*, 4642.
[25] Y.-Z. Long, M. Yu, B. Sun, C.-Z. Gu, Z. Fan, *Chem. Soc. Rev.* **2012**, *41*, 4560.
[26] S.-Y. Min, T.-S. Kim, B. J. Kim, H. Cho, Y.-Y. Noh, H. Yang, J. H. Cho, T.-W. Lee, *Nat. Commun.* **2013**, *4*, 1773.
[27] W. E. Teo, S. Ramakrishna, *Nanotechnology* **2006**, *17*, R89.
[28] Z.-M. Huang, Y.-Z. Zhang, M. Kotaki, S. Ramakrishna, *Compos. Sci. Technol.* **2003**, *63*, 2223.
[29] G. Xu, C. M. TorresJr., J. Bai, J. Tang, T. Yu, Y. Huang, X. Duan, Y. Zhang, K. L. Wang, *Appl. Phys. Lett.* **2011**, *98*, 243118.
[30] A. C. Ferrari, J. C. Meyer, V. Scardaci, C. Casiraghi, M. Lazzeri, F. Mauri, S. Jiang, D. Piscanec, K. S. Novoselov, S. Roth, A. K. Gein, *Phys. Rev. Lett.* **2006**, *97*, 187401.
[31] Z. Shi, R. Yan, L. Zhang, Y. Wang, D. Liu, D. Shi, E. Wang, G. Zhang, *Adv. Mater.* **2011**, *23*, 3061.
[32] L. R. Radovic, B. Bockrath, *J. Am. Chem. Soc.* **2005**, *127*, 5917.
[33] X. Jia, J. Campos-Delgado, M. Terrones, V. Meunier, M. S. Dresselhaus, *Nanoscale* **2011**, *3*, 86.
[34] X. Zhang, J. Xin, F. Ding, *Nanoscale* **2013**, *5*, 2556.
[35] F. Schwierz, *Nat. Nanotechnol.* **2010**, *5*, 487.
[36] J. Wang, R. Zhao, M. Yang, Z. Liu, Z. Liu, *J. Chem. Phys.* **2013**, *138*, 084701.
[37] Z. Cheng, Q. Zhou, C. Wang, Q. Li, C. Wang, Y. Fang, *Nano Lett.* **2011**, *11*, 767.
[38] Y.-C. Lin, C.-C. Lu, C.-H. Yeh, C. Jin, K. Suenaga, P.-W. Chiu, *Nano Lett.* **2012**, *12*, 414.
[39] J. W. Suk, W. H. Lee, J. Lee, H. Chou, R. D. Piner, Y. Hao, D. Akinwande, R. S. Ruoff, *Nano Lett.* **2013**, *13*, 1462.
[40] J. M. Yun, S. Park, Y. H. Hwang, E.-S. Lee, U. Maiti, H. Moon, B.-H. Kim, B.-S. Bae, Y.-H. Kim, S. O. Kim, *ACS Nano* **2014**, DOI: 10.1021/nn4053099.